OTA Throughput Prediction of MIMO Antennas for Wireless Devices by Simulated Realistic Channel Model

Xide Mei and Ke-Li Wu, *Fellow, IEEE*

***Abstract*— A cost-effective and accurate method for predicting over-the-air (OTA) data throughput of multiple-input and multiple-output (MIMO) wireless devices in the antenna design stage is proposed. The method incorporates passive characteristics of MIMO antennas, realistic channel model, and conductive measurement results in a computer simulation framework. With extracted relation between received power and signal-to-noise ratio (SNR) of a wireless device at antenna ports by a conductive test and measured passive characteristics of MIMO antennas, OTA throughput versus received power in a realistic channel model is obtained by the Monte Carlo simulation of Shannon's law. The unique features of this method include: no channel emulator equipment is required; a wide variety of precoding schemes can be applied; passive characteristics of antennas are fully incorporated; and frequency-selective fading channel can be adopted. The method has been intensively validated by comparing the calculated OTA throughputs with those measured by a multiprobe anechoic chamber method under spatial channel model extension (SCME) in three aspects: spatial correlation, radiation efficiency, and mutual coupling, showing as low as 0.2–0.3 dB discrepancy in power level in most cases. The method can be used to evaluate a MIMO array antenna design of a wireless device with respect to OTA performance.**

***Index Terms*— Device antennas, long-term evolution (LTE), multiple-input and multiple-output (MIMO), over the air (OTA) test, performance prediction, throughput.**

I. Introduction

IN A modern wireless device or user equipment (UE) such as a smartphone, the array antenna for accessing multiple-input and multiple-output (MIMO) scheme has become a compulsory module that decisively determines the data throughput in a multipath environment [1]. To assess the ultimate performance of a MIMO array antenna, the evaluation of over-the-air (OTA) data throughput of the wireless device equipped with the array antenna in a realistic channel environment, by either an experiment or simulation approach, is the necessary means for the developer. Therefore, various direct and indirect MIMO OTA measurement methods for evaluating the overall OTA performance of a MIMO wireless device with an array antenna have been proposed by the industry and academia.

Manuscript received 2 November 2021; revised 21 March 2022; accepted 22 May 2022. Date of publication 7 June 2022; date of current version 9 November 2022. This work was supported by the Postgraduate Scholarship of The Chinese University of Hong Kong. *(Corresponding author: Ke-Li Wu.)*

The authors are with the Department of Electronic Engineering, The Chinese University of Hong Kong, Hong Kong 999077 (e-mail: xdmei@link.cuhk.edu.hk; klwu@cuhk.edu.hk).

Color versions of one or more figures in this article are available at https://doi.org/10.1109/TAP.2022.3179524.

Digital Object Identifier 10.1109/TAP.2022.3179524

With years of effort, three MIMO OTA testing methodologies have been intensively investigated.

1) The reverberation chamber (RC) method [2], which was proposed for OTA test with an ideal rich isotropic multipath (RIMP) environment [3]. The RC method creates a Rayleigh-like fading channel for OTA measurement of a MIMO device with an omnidirectional distribution of angle of arrival (AOA). The RC method allows limited controlling of certain channel parameters such as coherence bandwidth by physically loading the RC with absorbing objects [4]. A comprehensive review of RC method is available in [5] and the solution of RC combined with channel emulator is also available in [6].
2) The multiprobe anechoic chamber (MPAC) method [7] that employs a multichannel spatial fading emulator (SFE), a communication tester (CT) for emulating a MIMO base station (BS), and multiple dual-polarized probes uniformly distributed on a circle ring for a two-dimensional (2-D) case and multiple circle rings for a three-dimensional (3-D) case inside an anechoic chamber. An MPAC OTA measurement system can reproduce a realistic channel environment according to the specified statistic channel model, such as the spatial channel model extension (SCME), which incorporates essential radio propagation parameters in both spatial and temporal domains [8]. The MPAC method is also a candidate method for 5G OTA measurement setup for frequency range one (FR1) and frequency range two (FR2) [9].
3) The two-stage method [7], [10], [11], with which the device under test (DUT) is either directly connected to the outputs of an SFE [10] or wirelessly connected to the outputs of an SFE [11], with which the signals are multiplied by the antenna radiation patterns through a sophisticated equipment setup. The radiated two-stage method proposed in [11] is further formulated and theoretically enhanced by the wireless cable method [12]. Similar to the MPAC method, the two-stage method also needs SFE equipment to multiply the signal from a CT with channel characteristics in real time.

It can be found that the existing MIMO OTA test methods require either expensive equipment for reproducing a realistic channel environment (methods 2 and 3) or an approximate hardware means to emulate a realistic channel model (method 1). To accommodate the increased demands for MIMO OTA test of the DUT mounted on vehicle, for which a physically emulated multipath channel environment is very difficult to reproduce, it is highly desirable to use computer-simulated realistic channel model. The relative strengths and weaknesses of five commonly used MIMO OTA test methods are compared in [13] recently. Another advantage of using simulated channel model is that it allows to use not only the measured but also electromagnetic (EM) simulated antenna gain patterns and port S-parameters. This feature permits antenna designers to evaluate the OTA performance while working on EM-based antenna models. In addition, since the channel model is fully computerized, upgrading the model and accommodating more sophisticated MIMO transmission modes (TMs) become very easy.

There is abundant literature dealing with performance evaluation of a MIMO system in a wireless channel based on the statistical analysis. Many papers work on evaluating the system performance of a terminal device by calculating the channel capacity with respect to the following:

1) different sorts of channel models, including realistic (i.e., SCME model [14] and WINNER II model [15]), and idealistic channel models (i.e., Rayleigh fading model [16] and Rician fading model [17]);

2) different types of TMs, such as diversity mode [18] and multiplexing mode [19];

3) the properties of the antenna characteristics, such as mutual coupling and radiation patterns [20].

A noticeable work to assess data throughput of a DUT in an isotropic-scattering idealistic Rayleigh fading channel model with statistic Monte Carlo simulation is reported in [21], in which the data throughput is obtained based on the outage theorems [22] in terms of statistic properties of the received power level. In the simulation model, only the envelope correlation coefficient (ECC) [23] of the terminal MIMO antenna is used to characterize the antennas. Although a multipath Kronecker channel model is considered for calculating the data throughput in [24], since the features of antennas are incorporated through ECC, the model is not sufficiently accurate as far as the passive characteristics of MIMO antennas are concerned.

In this article, a comprehensive and cost-effective method for predicting the OTA data throughput of a MIMO wireless device is proposed. The method is based on a simulated realistic channel model, the measured received power versus signal-to-noise ratio (SNR) relation of the onboard communication system of the DUT, and the measured or EM simulated antenna passive characteristics, including port S-parameters and 3-D radiated gain patterns of the wireless device, which are usually available at the hand in the antenna design stage. The method is analogous to the MPAC method but without requiring expensive hardware channel emulators and the anechoic chamber for hosting the multiple probes. The method is applicable to OTA throughput prediction in both 2-D and 3-D realistic channel models without requiring more resources. Since the simulated channel model is used and the data throughput is calculated based on Shannon's law, the channel profile, coding method, and MIMO TMs can be easily updated only in the simulation framework. Although the proposed framework does not incorporate the desense effect [25], the effect can be considered if the radiated two-stage method or wireless cable method [11], [12] is adopted. The proposed method is suitable for MIMO antenna designers to evaluate the impact of the designed MIMO antennas on system data throughput when the 3-D antenna gain patterns of MIMO antennas and the conduct test of the onboard system are already available.

Although intensive experimental validation through MPAC OTA tests is conducted using a 2 × 2 MIMO LTE module, it can be understood that the method is also applicable to other MIMO communication schemes. The side product is that the experimental tests provide a comprehensive design guideline about how antenna attributes affect the system data throughput from antenna designer point of view. The attributes include antenna spacing, mutual coupling, antenna radiation patterns, and radiation efficiency. The 2-D SCME channel model is chosen in simulation and experimental validation though there is no restriction to apply more advanced channel model such as the recently proposed 5G channel models [9].

This article starts with a brief review of MIMO antennas from the information theory perspective. Then, a general realistic SCME channel model with inclusion of antenna port characteristics is introduced and is followed by the procedure that maps the SNR to the received power level of the onboard system. The method is validated intensively in various aspects, including spatial correlation, antenna total efficiency, and the mutual coupling between two MIMO antennas. All the passive characteristics of sample antennas for validation are obtained experimentally. In most cases, the accuracy between the calculated and the measured power level is about 0.2–0.3 dB for typical throughput value, which is within the uncertainty of antenna gain measurement.

II. Evaluation Method

To facilitate the understanding of the method, the basic concepts of the statistic channel matrices that reflect the MIMO antenna port characteristics will be briefly reviewed before presenting the detailed OTA evaluation process.

A. System Model of MIMO Wireless Communications

Assume that the BS is in a transmitting (Tx) mode and the device is in the receiving (Rx) mode. Several data streams are formed between the MIMO antenna arrays of Tx and Rx through the wireless channel. In terms of different precoding and decoding methods, the mathematical representation of the outage channel capacity according to Shannon's law can be written as

$$C = B \times \log_2 \det\left(\mathrm{I} + \frac{\mathbf{U}^\dagger \mathbf{H}\mathbf{V}\mathbf{Q}\mathbf{V}^\dagger \mathbf{H}^\dagger \mathbf{U}}{\sigma^2}\right) \quad (1)$$

where B denotes the signal bandwidth, $\mathbf{V}$ is the precoding matrix, $\mathbf{U}$ is the decoding matrix, $\mathbf{I}$ is the identity matrix with the dimension of $N_r \times N_r$, $\mathbf{Q}$ is the signal power distribution on the transmitter side, σ^2 is the noise power, $\mathbf{H}$ is the complex-valued wireless channel matrix with the dimension of $N_r \times N_t$, det $(\cdot)$ denotes the determinant operation, and $(\cdot)^\dagger$ denotes the Hermitian transpose.

There are various precoding and decoding methods, such as SVD beamforming method [26], zero-forcing beamforming method [27], and minimum mean square error (MMSE) beamforming method [28]. In practice, there are several different TMs in the 3GPP standard [30]—TM-1–TM-10, where TM-2 (transmission diversity) and TM-3 (open-loop spatial multiplexing) are commonly used in the LTE signal transmission since, in most cases, the receiver has perfect knowledge of the channel, whereas the transmitter does not. For 5G communication system, the channel coding will be low-density parity check (LDPC) [31]. In the validation examples to be discussed in Section III, TM-3 MIMO TM, which uses zero-forcing precoding, is chosen in the CT.

B. Channel Matrices and Wireless Channel Model

A number of standardized channel models are available for evaluating a wireless communication system, e.g., the spatial channel model (SCM) [8], SCME [14], and the WINNER II model [15]. These models are originated from the SCM described in [32]. According to the measured results in various multipath environments, the extended tap-delay-line model is found to be most suitable for the general SCM [33], in which different taps present different signal transmission paths in terms of signal delays, directions of incoming and outgoing waves, and the complex channel coefficient. Mathematically, the transfer function between the ith transmitting antenna and the jth receiving antenna in the channel matrix $\mathbf{H}_N(\tau, t)$ can be expressed as [8]

$$H_{N,ij}(\tau; t; \Theta) = \sum_n \sum_m a_{mn,ij}(t)\delta\big(\tau - \tau_{mn,ij}\big)\delta\big(\Theta - \Theta_{mn,ij}\big) \tag{2}$$

in which

$$\begin{aligned} &a_{mn,ij}\big(\theta_{AOD,mn}, \theta_{AOA,mn}, t\big) \\ &\quad= \begin{bmatrix} \sqrt{G_{vi}\big(\theta_{AOA,mn}\big)}e^{j\varphi_v(\theta_{AOA,mn})} \\ \sqrt{G_{hi}\big(\theta_{AOA,mn}\big)}e^{j\varphi_h(\theta_{AOA,mn})} \end{bmatrix}^T \\ &\qquad\times \begin{bmatrix} h_{vv}\big(\theta_{AOD,mn}, \theta_{AOA,mn}\big) & h_{vh}\big(\theta_{AOD,mn}, \theta_{AOA,mn}\big) \\ h_{hv}\big(\theta_{AOD,mn}, \theta_{AOA,mn}\big) & h_{vv}\big(\theta_{AOD,mn}, \theta_{AOA,mn}\big) \end{bmatrix} \\ &\qquad\times \begin{bmatrix} \sqrt{G_{vj}\big(\theta_{AOD,mn}\big)}e^{j\varphi_v(\theta_{AOD,mn})} \\ \sqrt{G_{hj}\big(\theta_{AOD,mn}\big)}e^{j\varphi_h(\theta_{AOD,mn})} \end{bmatrix} \\ &\qquad\times \exp\big(jkv\cos\big(\theta_{m,n,AOA} - \theta_v\big)t\big) \end{aligned} \tag{3}$$

where m is the index of the mth subpath within the nth cluster, θ_{AOA} is the angle of arrival, θ_{AOD} is the angle of departure, and τ is the delay. In (3), h_{vv}, h_{vh}, h_{hv}, and h_{hh} are the vertical-to-vertical, vertical-to-horizontal, horizontal-to-vertical, and horizontal-to-horizontal transmission coefficients, respectively; G_v and G_h are the scalar antenna gains of vertical and horizontal components, respectively; φ_v and φ_h are the phases of the vertical and horizontal components of the field, respectively; v is the velocity of the wireless devices; and θ_v is the moving direction of the wireless device. All the variables described here are random variables and their distributions are carefully described in [8]. It should be noted that the phase difference between two received signals due to the displacement of antennas is explicitly expressed. In particular, the phase information of antenna radiation pattern as well as the phase difference due to the displacement are reflected in φ_v and φ_h of each of MIMO antennas, provided that the coordinate system for measuring the radiation pattern of each antenna is the same as that for the OTA test. It needs to be noted that the channel matrix $\mathbf{H}_N(\tau, t)$ is established under the assumption that the mutual coupling is negligible. The open-source code for implementing (2) and (3) can be found in [34] except for the phase terms φ_v and φ_h.

TABLE I

SPECIFICATIONS OF UMI SCENARIO IN THE SCME CHANNEL MODEL

Specification of Umi scenario								
Cluster	Delay/ns			Fading/dB			AOD/°	AOA/°
1	0	5	10	-3	-5.2	-7	6.6	0.7
2	285	290	295	-4.3	-6.5	-8.3	14.1	-13.2
3	205	210	215	-5.7	-7.9	-9.7	50.8	146.1
4	660	665	670	-7.3	-9.5	-11	38.4	-30.5
5	805	810	815	-9	-11	-13	6.7	-11.4
6	925	930	935	-11	13.6	-15	40.3	-1.1

Other Parameters

Parameters	Value
Delay Spread	294 ns
Cluster Angular Spread(AOD) /Cluster Angular Spread(AOA)	5°/35°
Power Angular Distribution	Laplacian
Overall Angular Spread(AOD) /Overall Angular Spread(AOA)	18.2°/67.8°
Speed/Direction	30km/h / 120°

To obtain the channel capacity at a statistic sample in time t of the channel matrix using (1), the frequency-dependent quasi-static wideband channel model [35] is assumed and the channel matrix $\mathbf{H}_N(\tau, t)$ described in (2) can be inversed to the frequency domain $\mathbf{H}_N(f, t)$ using the Fourier transformation in the delay domain [36].

Although the proposed method is general for a 3-D realistic channel model, without any loss of generality, the 2-D ray-based SCME channel model is used to validate the method for two reasons: it is one of the recommended models by cellular telecommunications industry association (CTIA) for OTA test and it can be experimentally validated in the SATIMO MIMO-H 16-probe channel emulator. In the stage of Monte Carlo simulation, different channel matrices can be generated according to the SCME channel model described in [7].

The commonly used three scenarios in the SCME channel model are: urban micro (Umi) model, urban macro (Uma) model, and suburban micro model. In this work, Umi scenario, whose specification is listed in Table I, is selected as the channel model to validate the proposed method.

To reflect the attributes of the array antenna on the DUT accurately in evaluating the OTA data throughput, antenna mutual coupling among MIMO antennas must be incorporated into the mathematic model. Assume that the MIMO antennas on the Tx side are well matched and mutual coupling is negligible, and it can be found that the channel matrix without considering the mutual coupling $\mathbf{H}_N(f,t)$ and the actual channel matrix $\mathbf{H}(f,t)$ that involves mutual coupling on an MIMO wireless device are related to the characteristic matrix $\mathbf{K}_R$ by [20]

$$\mathbf{H}(f,t) = (\mathbf{I}+\mathbf{K}_R)\mathbf{H}_N(f,t), \quad \text{with } \mathbf{K}_R = \mathbf{C}_{R,12}\left(\mathbf{C}_{R,11}\right)^{-1} \quad (4)$$

where $\mathbf{C}_{R,11}$ is a diagonal matrix that is associated with input impedance of MIMO antennas versus frequency, whereas $\mathbf{C}_{R,12}$ incorporates the mutual coupling of the MIMO antennas and is complementary to $\mathbf{C}_{R,11}$ by extracting all the off-diagonal matrix elements such that

$$\mathbf{Z}_0(\mathbf{Z}_0+\mathbf{Z})^{-1} = \mathbf{C}_{R,11}+\mathbf{C}_{R,12} \quad (5)$$

where $\mathbf{Z}$ is the impedance matrix of the MIMO antenna elements and $\mathbf{Z}_0$ is a diagonal matrix representing the reference port impedance of the antennas, which is set to 50 Ω in this study. Note that the impedance matching condition of the MIMO antennas on the terminal side has been reflected in $\mathbf{H}_N(f,t)$ through the measured gain patterns and that the mutual coupling effect of the MIMO antenna of the wireless device is incorporated in the characteristic matrix $\mathbf{K}_{\mathrm{R}}$.

Since the SCME model is a wideband channel model, the signal bandwidth B can be divided into N_f subcarrier bands, and the total channel capacity can be rewritten as

$$C(t) = \sum_{n_f=1}^{N_f} B_{sub} \times \log_2 \det\left[\mathbf{I} + \frac{\gamma}{N_t}\mathbf{U}^\dagger \mathbf{H}\left(f_{n_f},t\right)\mathbf{H}^\dagger\left(f_{n_f},t\right)\mathbf{U}\right] \quad (6)$$

where B_{sub} is the bandwidth of subcarrier band and $\mathbf{H}(f_{n_f},t)$ is the channel matrix at the n_fth subcarrier frequency of sampling time t.

C. Received Power Versus SNR

It is known that the channel capacity sets the upper bound of the data rate of a given channel subject to a specific signal-to-noise ratio (SNR or γ) of a communication system. In practice, however, γ is determined by many factors, such as the modulation scheme, the encoding/decoding scheme, the losses in the radio frequency (RF) circuit chain, and the signal power level reaching at the antenna port among many others. All these factors are related to the onboard communication system and are difficult to simulate or estimate. Obviously, the absolute data throughput versus power level at the antenna ports can be measured when the channel between Tx and Rx is set to all-pass mode. This measurement is called conductive test, by which the onboard communication system is directly connected to a CT by RF cables without intervention of a channel emulator or fading simulator. Fig. 1 shows the setup for a conductive test of 2 × 2 MIMO wireless onboard system.

Since the proposed method is general for any number of antennas, for demonstration purpose, without lose of generality, a 2 × 2 MIMO system is considered in the discussion. In measuring the highest data throughput versus power level by conductive test, the maximum data rate of the Tx mode on the CT, which emulates the MIMO BS, is varied according to the modulation and coding scheme (MCS) index under the same modulation scheme. For 16 QAM (quadrature amplitude modulation), its MCS index ranges from 10 to 15. Table II lists the maximum data rate of different MCSs under 16 QAM.

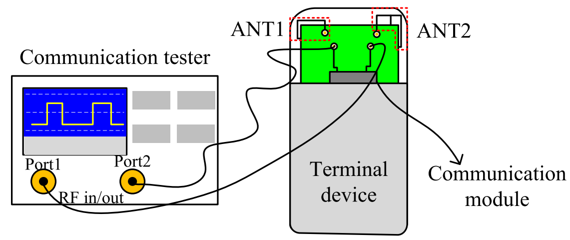

Fig. 1. Setup for conductive test of a 2 × 2 MIMO wireless device.

TABLE II
MAXIMUM DATA RATE OF DIFFERENT MCS INDEXES FOR 16 QAM 2 × 2 MIMO

MCS	10	11	12	13	14	15
Max. data rate (Mbps)	14.386	15.614	17.458	19.916	22.334	24.178

To illustrate the conductive test procedure, a commercial 2 × 2 MIMO module Huawei ME909 is used to mimic a MIMO wireless device. The module is connected to a Rohde & Schwarz CMW 500 CT through a pair of high-quality RF cables. No channel emulator is needed in the conductive test. As shown in Fig. 1, the communication module is disconnected from the MIMO antennas on the wireless device and is directly connected to the CT. The cable loss needs to be calibrated before the test and the additional phases of the two cables are set equal.

To find the relation between the received power level at the antenna port and the corresponding SNR (γ) of an onboard system, the following steps are performed.

Step 1: Choose an MCS index and set the Tx power, which equals the received power in the conductive test since the channel property in the conductive test is ideally all-pass by nature, high enough so that the data rate of the received signal reaches the maximum data rate of the chosen MCS.

Step 2: Gradually reduce the Tx power until the data rate of the received signal reaches 0. Having marked the “knee point” of the power level at which the data rate starts to decline as P_1 and the power level at which the data rate just reaches 0 as P_2, one can find the threshold power $\mathrm{P}_{\mathrm{thr}}$ for the MCS by taking the arithmetic average of P_1 and P_2.

Step 3: Repeat steps 1 and 2 for all the MCS indices of interest. The threshold power $\mathrm{P}_{\mathrm{thr}}$ for each of the MCS indices is obtained. The measured conductive data throughput versus received power for different MCS indices is shown in Fig. 2(a).

Step 4: Calculate the capacity versus SNR (γ) by (1) with the channel matrix set to the identity matrix. The dashed line in Fig. 2(b) presents the capacity versus γ for the 2 × 2 MIMO module when the signal bandwidth B is set to 10 MHz. This curve can be reused for any 2 × 2 MIMO system in the same frequency band.

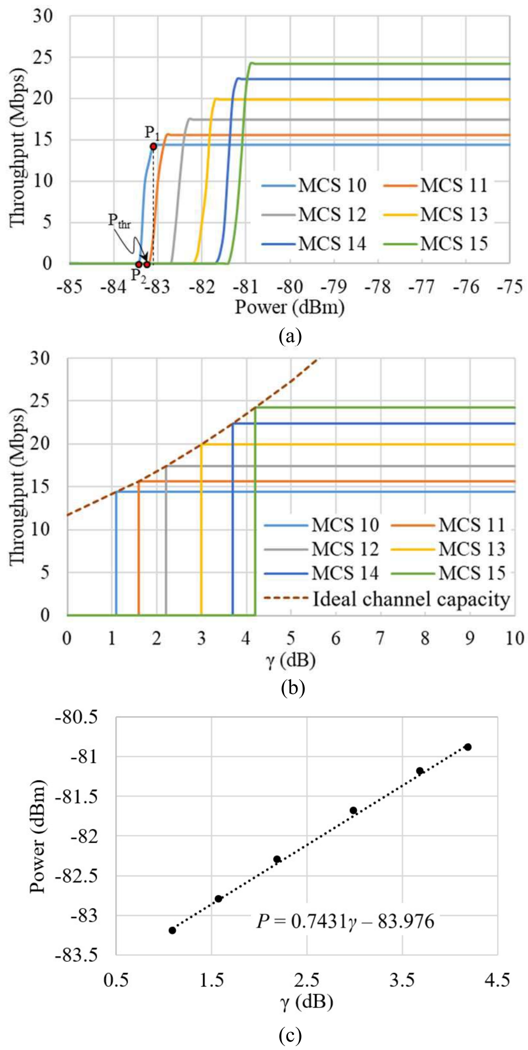

Fig. 2. Characteristics of data throughput, received power level, and SNR of onboard system. (a) Measured conductive throughput versus received power. (b) Calculated throughput versus SNR with idealistic identity channel matrix. (c) Extracted power of received signal versus SNR.

Step 5: Denote the threshold SNR (γ_{thr}) for a given MCS by finding the x-coordinate of the intersect of the constant maximum data rate of the MCS and the dashed line curve obtained in Step 4. Fig. 2(b) shows the threshold SNR for different MCS indices. It has been observed that idealistic step functions observed in Fig. 2(b) resemble the measured throughput versus power curves of the conductive test shown in Fig. 2(a).

Step 6: Associate threshold power P_{thr} and threshold SNR (γ_{thr}) of the same MCS. The relation between SNR and power level (P) of the received signal can be written as

$$P[\text{dBm}] = f(\gamma) + \Delta \tag{7}$$

where $f(\cdot)$ is a function to be curve-fitted and Δ is an error term that may be caused by the desense effect of the onboard system caused by the radiation of MIMO antennas.

The desense effect is caused by EM interference among electronic modules on the board and needs to be carefully minimized to a low level in a modern wireless device. In most cases, the function $f(\cdot)$ for a given wireless device can be well fitted by a linear function. In this demonstration example, the relation can be found as

$$P[\text{dBm}] = 0.7431\gamma - 83.976 \tag{8}$$

which is sketched in Fig. 2(c).

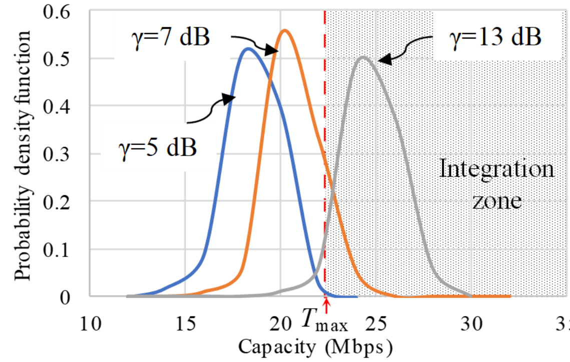

Fig. 3. Probability density function of channel capacity in a realistic channel model for different SNRs.

D. Statistic Model for OTA Throughput Evaluation

In general, OTA data throughput is the data rate at which a reliable communication measured specified by a given maximum bit error rate (BER) is achieved. As shown in Fig. 2(a), the throughput drops drastically when signal input power is lower than a threshold value. The rationale behind is that if the data capacity is lower than the maximum data rate in a certain extent, communication becomes impossible. In other words, the OTA data throughput T_{OTA} is proportional to the probability that the channel capacity C is equal or larger than the maximum data rate $T_{\max}$ of the signal with given SNR (γ). Mathematically

$$T_{OTA} = T_{\max} \int_{T_{\max}}^{\infty} \text{pdf}(C, \gamma)\, dC \tag{9}$$

where pdf $(\cdot)$ is the probability density function (PDF) of the channel capacity for a given SNR. Equation (9) is called threshold receiver model for evaluating throughput of wireless devices in an RC [37], in which a Rayleigh fading environment is considered. Fig. 3 shows three typical PDFs versus SNR. The detailed steps for simulating the OTA data throughput by a Monte Carlo analysis are summarized as follows.

Step 1: Acquire the passive characteristics of the MIMO antennas, including vector radiation gain patterns for both polarizations (in dBi) and impedance matrix $\mathbf{Z}$ experimentally or by EM simulation. For a system with a wide carrier bandwidth, the passive characteristics need to be measured at multiple frequencies.

Step 2: Conduct conductive test to obtain the relation in (7), from which the range of γ for the given power range of interest can be found.

Step 3: Sample the channel matrix $\mathbf{H}_N(\tau, t)$ in time t through (2) and (3) to generate the channel matrix in time and delay domains for which the radiation patterns obtained in step 1 are applied, and transform the channel matrix from the delay domain to the frequency domain $\mathbf{H}_N(f,t)$ according to [36].

Step 4: Sample $\mathbf{H}_N(f,t)$ at 18 subcarriers within the signal frequency band for SCME channel models, ensuring that each subchannel experiences flat fading, at each of which the narrowband channel matrix is obtained.

Step 5: Find $\mathbf{H}(f_{nf},t)$ from $\mathbf{H}_N(f_{nf},t)$ using (4).

Step 6: Obtain the matrix $\mathbf{U}$ and $\mathbf{V}$ from $\mathbf{H}(f_{nf},t)$ for each subcarrier at sampling time t. For a 2×2 MIMO system using zero-forcing decoding, which is used for validation examples, the matrix $\mathbf{U}$ and $\mathbf{V}$ can be found as

$$\mathbf{U} = \mathbf{H}^{\dagger}(f_{nf},t)\left[\mathbf{H}(f_{nf},t)\mathbf{H}(f_{nf},t)^{\dagger}\right]^{-1}\eta, \mathbf{V}=\mathbf{I}$$

where

$$\eta = \begin{bmatrix} 1/\eta_1 & 0 \\ 0 & 1/\eta_2 \end{bmatrix},$$

$$\eta_i = \sqrt{\left\{\left[\mathbf{H}(f_{nf},t)\mathbf{H}(f_{nf},t)^{\dagger}\right]^{-1}\right\}_{ii}} \quad i = 1 \text{ or } 2$$

and $\{\cdot\}_{ii}$ represents the entry of the ith column and the ith row of the matrix.

Step 7: Sweep γ in the range to calculate the corresponding channel capacity C with (6) for each time sample t.

Step 8: With the statistic channel capacity data versus γ obtained in steps above, find the PDF of the channel capacity versus γ, with which the data throughput T_{OTA} versus γ can be obtained using (9).

Step 9: Transform γ to the received power P by (8) to obtain the data throughput versus received power.

The Monte Carlo analysis is conducted by repeating Steps 3–7 in the time domain by sampling t in (2) and (3). In the validation example, 5000 time samples with time interval $\Delta t = c/4vf_c$ (f_c is the center frequency of the downlink signal and c is the velocity of light) are taken according to the 3GPP protocol [38] for each subcarrier.

It can be seen that there are multiple advantages by numerically finding PDF: 1) it allows the adoption of a realistic channel model that is usually not available in a closed form; 2) it permits flexibly emulating a wide variety of MIMO precoding and diversity schemes; 3) it can incorporate realistic port characteristics of the MIMO antennas; and 4) it enables evaluation of data throughput of a wireless device in a wideband or frequency-selective fading channel.

III. Experimental Validation

In this section, three experimental tests are presented in three aspects: spatial correlation due to antenna placement, radiation efficiency, and mutual coupling level. The concerned antenna attributes are obtained by passive measurements. Each experiment is prepared in such a way that only one attribute is varied, while others remain unchanged. The numerically calculated OTA data throughputs are fully verified by corresponding experiments using the MPAC method, for which the same channel model and parameters as those of the numerical evaluation are used. The experimental results also serve as design guidelines for MIMO antennas of wireless devices.

Fig. 4. Connection of two MIMO antennas with a TD-LTE data communication module for experimental validation.

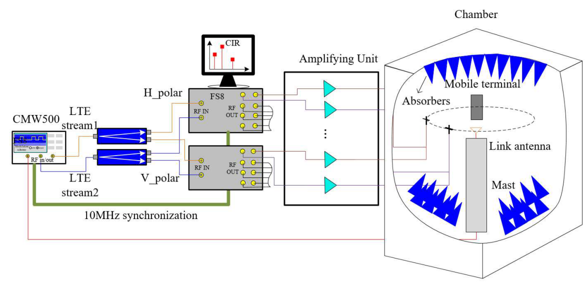

Fig. 5. OTA measurement setup using multiprobe-based multipath channel emulator.

A. Experimental Setup

All the sample antennas are fabricated on an FR4 PCB board that is with a relative permittivity of 4.6, a thickness of 1 mm, and a loss tangent of 0.015. The commercial TD-LTE data communication module of ME909 is used to emulate an onboard 2×2 MIMO communication system of a wireless device. The passive characteristics of sample antennas are measured and utilized in data throughput calculation. Each antenna on the PCB board is fed by a coplanar waveguide transmission line that is connected to the MIMO module through a short RF cable, as shown in Fig. 4. The communication module supports the 2×2 MIMO scheme in LTE bands 1, 3, and 7. Nevertheless, the operating frequency of the three examples is set to LTE band 3 (1805–1880 MHz) with a signal bandwidth of 10 MHz.

The experimental setup of the in-house SATIMO MIMO-H system [39] is shown in Fig. 5, in which two streams of LTE signal are generated from Rohde & Schwarz CMW 500 CT [40]; the LTE signal passes through two synchronized sets of eight-channel Anite FS8 channel emulators that modulate the data streams with the chosen realistic channel information; the modulated signals are then sent to eight dual-polarized probes that are uniformly distributed on the horizontal circle ring in an anechoic chamber to emulate a multipath environment [41]; the transmitted signal is received by the wireless DUT that is placed at the center of the circle; and the DUT feedbacks to CT for monitoring the BER. The statistic characteristic of the channel model realized by the in-house SATIMO MIMO-H system is fully validated according to the protocol given in [7]. The largest error in the

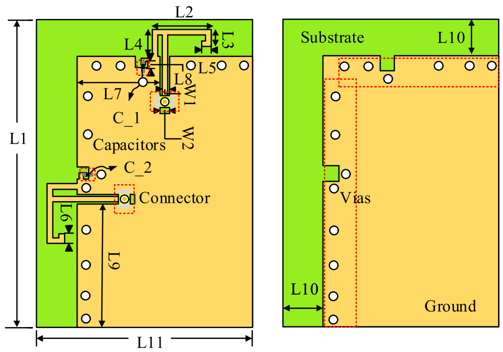

(a) (b)

Fig. 6. Dimensions of antenna samples for validating throughput with different spatial correlations. Capacitors C_1 and C_2 are inlaid in two notches for controlling mutual coupling. (a) Antenna layout (front). (b) Antenna layout (back).

TABLE III

ANTENNA DIMENSIONS AND CAPACITORS FOR DIFFERENT SPATIAL CORRELATION ARRANGEMENTS

Dimensions (Unit: mm)	L1	L2	L3	L4	L5	L6	L7	L8
	140	23.1	4.1	7.5	2.4	3.9	28.7	2.9
	L10	L11	W1	W2				
	8	75	1.1	1.6				
	L9							
	Case a		*Case b*		*Case c*		*Case d*	
	99.2		84.2		69.2		54.2	
Capacitors (Unit: pF)	*Case a*		*Case b*		*Case c*		*Case d*	
	C_1	C_2	C_1	C_2	C_1	C_2	C_1	C_2
	3.6	3.9	3.6	3.7	3.7	3.9	3.6	3.7
Distance (Unit: λ)	*Case a*		*Case b*		*Case c*		*Case d*	
	0.33		0.4		0.46		0.58	

power reception of the six clusters is less than 0.3 dB, showing a very good control of channel statistic properties. Because both CT and the communication module support two-channel MIMO tests, the validation is limited to 2 × 2 MIMO cases. All experiments are measured in the Umi SCME channel model and the measured data throughput is an average of the measured throughput values by rotating the DUT for every 45° in the horizontal plane. The calculated data throughput using the proposed method follows the same rotation arrangement. The conductive throughput for each MCS index of the communication module is measured as shown in Fig. 2(a), from which the power versus SNR relation plotted in Fig. 2(c) is extracted.

B. Experiment 1: Throughput Versus Spatial Correlation

It is known that the spatial correlation of MIMO antennas will significantly affect the data throughput from the communication theory point of view. However, on the antenna design side, spatial correlation not only depends on the relative position of MIMO antennas but also on the radiation patterns. This concept is well revealed by (2) and (3), where the channel capacity is only affected by the gain and phase patterns of MIMO antenna.

In this experiment, four sets of sample MIMO antenna arrays are prepared. The layout of sample antennas is shown in Fig. 6(a) and (b). In order to observe the influence of spatial correlation without influence of mutual coupling, the self-curing decoupling technique [42] is used to maintain mutual coupling at a sufficiently low level. Four samples are prepared by fixing dimension "L7" and varying dimension "L9" along the long edge of the circuit board. The detailed dimensions of the four samples are given in Table III. The center-to-center antenna distance is measured in the terms of free-space wavelength according to the definition in the CTIA MIMO OTA test plan [7].

The measured reflection coefficients for all antenna samples in this experiment are less than −15 dB and mutual coupling levels are less than −25 dB within the operating frequency band. The magnitudes of radiation patterns of the four samples are almost in the same shape with less than 0.5 dB variation in the maximum gain. The PDF for each case of antenna sample with all rotation arrangements is generated with the antenna radiation patterns and the port S-parameters measured at 1855 MHz. The calculated OTA throughput versus the received power for each sample array antenna of different MCS indices is shown in Fig. 7(a)–(f). The measured OTA throughputs obtained with the same channel model and MCS indices are also superimposed in Fig. 7, showing very good agreement with the calculated ones. It is demonstrated that when the antenna spacing is decreased from 0.58 wavelength to 0.3 wavelength, the OTA throughput will drop by about 0.5 dB in terms of received power level.

C. Experiment 2: Throughput Versus Antenna Total Efficiency

Needless to say, antenna total efficiency decisively determines the OTA performance. However, to what degree of efficiency degradation the throughput is acceptable will require a comprehensive assessment of OTA performance. Such an assessment can be done easily by the proposed evaluation method.

To investigate the influence of total efficiency on OTA throughput, a small piece of lossy material is stuck to the back of each antenna sample to independently alter the radiation efficiency without affecting the matching efficiency and radiation patterns noticeably. The commercial absorber material ECCOSORB SS3 tape [43] with a thickness of 1/8 in is chosen. In the experiment, the mutual coupling is reduced to a significantly low level using the self-curing decoupling technique. The layouts of the antenna samples are presented in Fig. 8(a) and (b). For comparison purpose, four pieces of MIMO antenna samples of the same layout but with different sizes of lossy materials are prepared to realize different radiation efficiencies. The dimensions of antennas and the sizes of lossy materials are listed in Table IV.

Having acquired the antenna passive characteristics by experiment and conductive test results, the OTA data throughputs of the LTE module equipped with four different MIMO antenna samples can be calculated by the Monte Carlo simulation with 40 000 samples. The calculated results are further verified by the measured OTA throughput for different MCS indices. The total efficiency of each antenna sample is

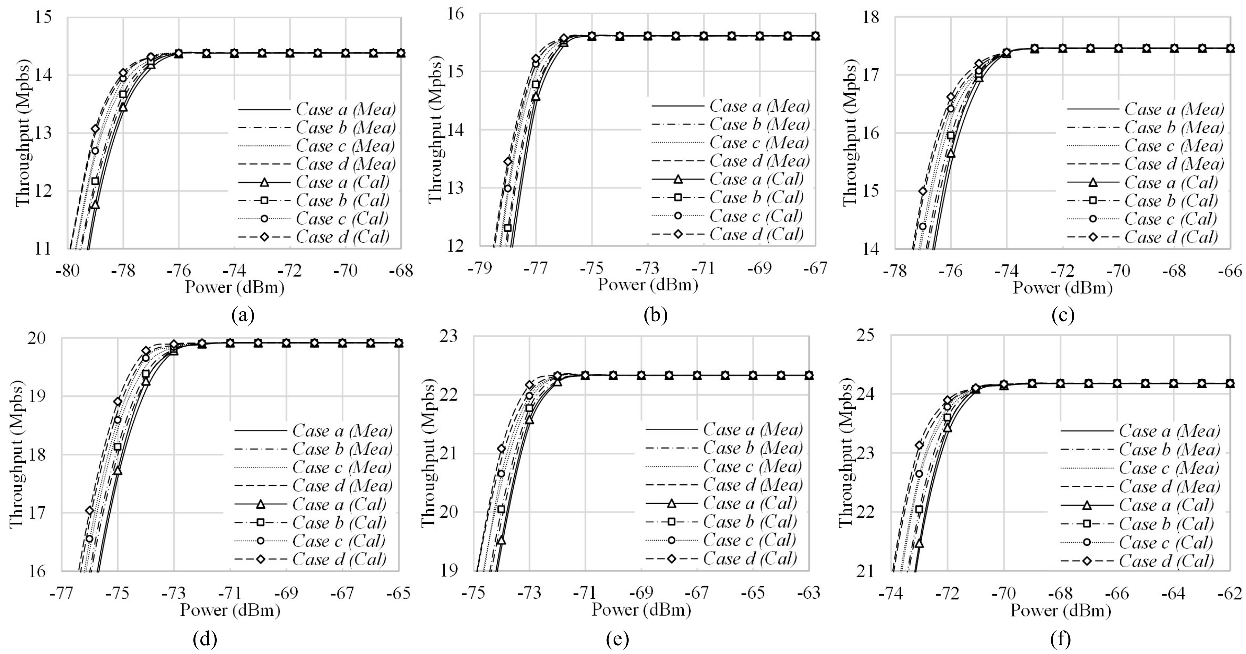

Fig. 7. Measured and calculated OTA data throughputs for different antenna element spacing. (a)–(f) MCS 10, 11, 12, 13, 14, and 15, respectively.

TABLE IV

DIMENSIONS FOR ANTENNA SAMPLES OF DIFFERENT TOTAL EFFICIENCIES (CAPACITOR C = 3.3 pF)

Dimensions (Unit: mm)	L1	L2	L3	L4	L5	L6	L7	L8
	140	75	7.5	20.6	4.1	8.9	2.5	2
	L9	L12	W1	W2				
	8	21.7	1.1	1.6				
Absorber dimensions (Unit: mm)	*Case e*		*Case f*		*Case g*		*Case h*	
	L10	L11	L10	L11	L10	L11	L10	L11
	0	0	4.5	6	7.2	6.5	11.5	6.5

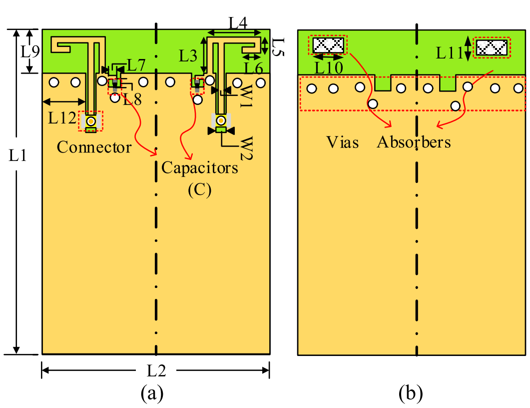

Fig. 8. Two element MIMO antenna array for investigating OTA throughput versus antenna total efficiency and mutual coupling. (a) Antenna layout (front). (b) Antenna layout (back).

measured and is shown in Fig. 9 with the frequency band of interest shaded. The total efficiency in this experiment ranges from 35% to 80%, which covers most of the practical cases for wireless device antennas. For all the four samples, the measured coupling levels are less than −20 dB and

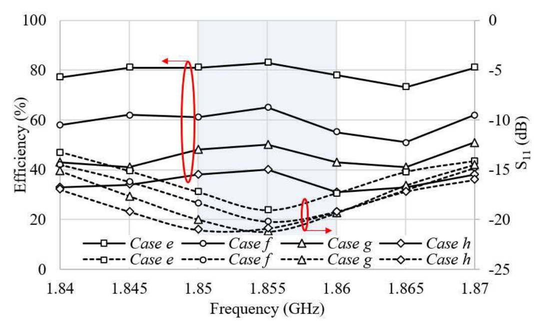

Fig. 9. Measured total efficiency and matching condition of four antenna samples for experiment 2.

the reflection coefficients are less than −15 dB within the operating frequency band, which are also superimposed in Fig. 9. By making use of the measured passive characteristics of the MIMO antennas, as well as the conductive throughput versus received power relation shown in Fig. 2(c), PDFs of the four MIMO antenna samples are calculated by the Monte Carlo simulation with 40 000 statistic samples. The calculated OTA data throughputs for the four cases at different MCS indices are presented in Fig. 10(a)–(f). The measured OTA throughputs are also superimposed in Fig. 10(a)–(f). Again, the calculated OTA throughputs are in good agreement with the measured in all cases. It can be observed that the required received power level needs to be increased by more than 2.5 dB if the total efficiency is decreased from 80% to 35%. This observation justifies that antenna efficiency is more dominating on OTA throughput than antenna spacing.

D. Experiment 3: Throughput Versus Mutual Coupling

It is well known that mutual coupling degrades SNR, desensitizes the receivers, and lowers the antenna radiation

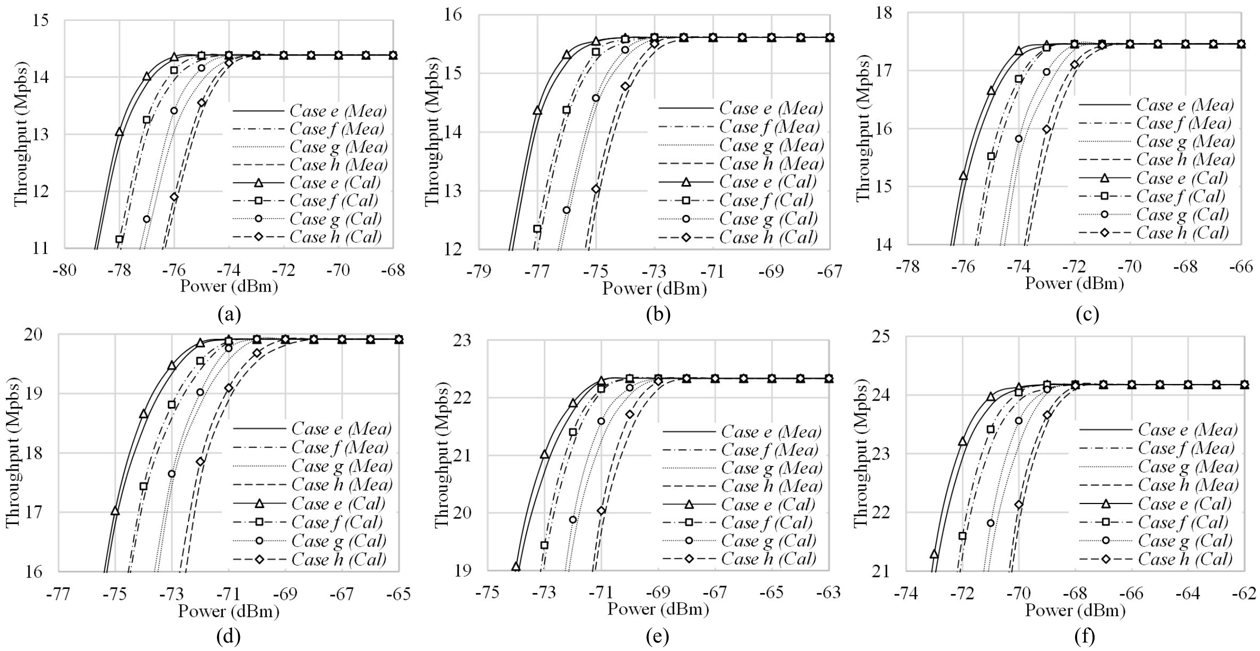

Fig. 10. Measured and calculated throughput for different antenna total efficiencies. (a)–(f) MCS 10, 11, 12, 13, 14, and 15, respectively.

TABLE V

ANTENNA DIMENSIONS AND CAPACITORS FOR DIFFERENT COUPLINGS

Dimensions (Unit: mm)	L1	L2	L3	L4	L5	L6	L7	L8
	140	75	7.5	20.6	4.1	8.9	2.5	2
	L9	L10	L11	L12	W1	W2		
	8	0	0	21.7	1.1	1.6		
Capacitor (Unit: pF)	*Case i*		*Case j*		*Case k*		*Case l*	
	3.2		3		2		0	

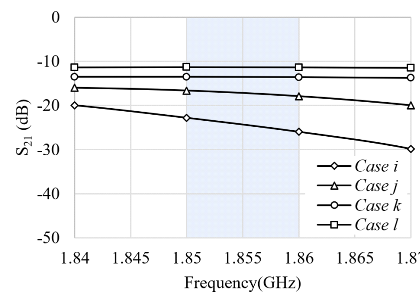

Fig. 11. Measured mutual coupling S21 of four measurement antenna samples for experiment 3.

efficiency [44], [45]. It is shown in (4) and (5) that mutual coupling between MIMO antennas has been incorporated in the channel matrix **H**. To verify the proposed method in assessing the impact of mutual coupling, four MIMO antenna samples are prepared on PCB boards. Each antenna pair is with fixed antenna spacing but different mutual coupling levels controlled by the decoupling capacitor. The layout of the sample antennas for investigating the mutual coupling impact is the same as those for the antenna efficiency, which is shown in Fig. 8, except that the absorbing material is removed. The dimensions of the sample antennas and decoupling capacitance are listed in Table V. The measured S_{21} in decibels for each pair of sample MIMO antennas is presented in Fig. 11 with variation from -23 to -11 dB. In all cases, the measured reflection coefficients are less than -15 dB within the operating frequency band. It is worth mentioning that the antenna total efficiency varies from 69% to 79% with the variation of mutual coupling level.

With the same procedure, the OTA data throughputs of the LTE module with the four MIMO antenna array samples can be calculated by the Monte Carlo simulation with 40 000 samples. The calculated results are further verified by the measured OTA throughput by the MPAC method. Both calculated and measured OTA throughputs are superimposed in Fig. 12, showing very good agreement. It can be observed that the required power level is decreased by more than 1.3 dB if the antenna coupling is decreased from -11 to -23 dB. This significant enhancement is partially contributed by the radiation efficiency improvement with the reduction of mutual coupling and signal correlation brought by mutual coupling.

Having presented the three validation cases, it can be concluded that the antenna radiation efficiency is more dominating to the received power than mutual coupling, whereas the antenna mutual coupling is more sensitive than the antenna spacing. In most of the cases shown in Fig. 12, the discrepancy between the calculated and the measured power level is about 0.2–0.3 dB for a typical throughput value, which is within the uncertainty of antenna gain measurement. The discrepancy may be partially attributed to the desense effect of the LTE module and the discrepancy in the channel models used in the calculation and measurements. It is advised that to obtain accurate passive characteristics of the antennas either by measurement or EM simulation, the antenna prototype, including its surrounding, needs to be prepared as close to

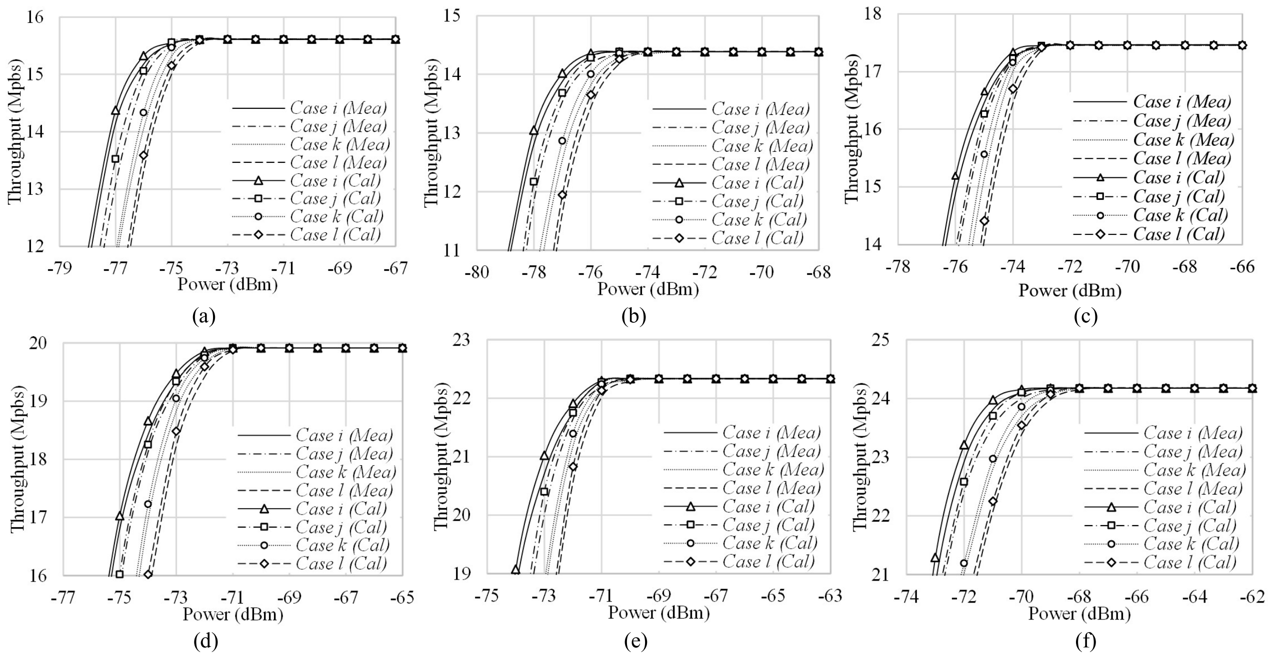

Fig. 12. Measured and calculated OTA throughput for different antenna mutual couplings. (a)–(f) MCS 10, 11, 12, 13, 14, and 15, respectively.

the actual environment as possible and that the desense effect in the actual wireless device should be minimized.

IV. Conclusion

This article presents a comprehensive, accurate and cost-effective scheme to predict OTA data throughput directly from the conductively measured throughput of the onboard system, complex vector antenna radiation patterns, and *S*-parameters among MIMO antenna ports of DUT. Since the proposed method is based on an off-line computation, antenna attributes can be acquired either from antenna passive measurements or EM simulation. The significance of this work is fourfold: passive characteristics of MIMO antennas are fully incorporated, no channel emulator equipment is required, it is applicable to assess the OTA performance in both 2-D and 3-D channel models, and no expensive equipment is required.

The proposed method is fully validated by the MPAC method under the Umi SCME channel model in three major aspects of MIMO antenna properties: antenna element spacing, antenna radiation efficiency, and mutual coupling. The influence of matching condition is reflected in the aspect of antenna total radiation efficiency. The calculated OTA throughputs in all aspects are in very good agreement with those of OTA measurements, which not only demonstrates the accuracy and usefulness of the proposed scheme but also provides fruitful design guidelines for MIMO antenna designers. This article, for the first time, thoroughly investigates how MIMO antenna spacing, mutual coupling, and antenna total efficiency affect the overall OTA performance of a wireless device from both the theoretical and the experimental aspects.

References

[1] M. A. Jensen and J. W. Wallace, "A review of antennas and propagation for MIMO wireless communications," *IEEE Trans. Antennas Propag.*, vol. 52, no. 11, pp. 2810–2824, Nov. 2004.

[2] D. Hill, "Electromagnetic theory of reverberation chambers," NIST, Boulder, CO, USA, Tech. Rep. 1506, Dec. 1998.

[3] P. S. Kildal and K. Rosengren, "Correlation and capacity of MIMO systems and mutual coupling, radiation efficiency, and diversity gain of their antennas: Simulations and measurements in a reverberation chamber," *IEEE Commun. Mag.*, vol. 42, no. 12, pp. 104–112, Dec. 2004.

[4] X. Chen, P. S. Kildal, C. Orlenius, and J. Carlsson, "Channel sounding of loaded reverberation chamber for over-the-air testing of wireless devices: Coherence bandwidth versus average mode bandwidth and delay spread," *IEEE Antennas Wireless Propag. Lett.*, vol. 8, pp. 678–681, 2009.

[5] P. S. Kildal, C. Orlenius, and J. Carlsson, "OTA testing in multipath of antennas and wireless devices with MIMO and OFDM," *Proc. IEEE*, vol. 100, no. 7, pp. 2145–2157, Jul. 2012.

[6] C. S. P. Lötbäck, A. Skårbratt, and C. Orlenius, "Extending the reverberation chamber using a channel emulator for characterisation of over-the-air performance of multiple-input-multiple-output wireless devices," *IET Sci., Meas. Technol.*, vol. 9, no. 5, pp. 555–562, Aug. 2015.

[7] (May 2018). *Test Plan for 2×2 Downlink MIMO and Transmit Diversity Over-the-Air Performance*. CTIA, Version 1.2. [Online]. Available: https://api.ctia.org/

[8] *Spatial channel model for mimo simulations*, 3GPP, document 25.996, V6.1.0, Jun. 2007.

[9] *Study on Radiated Metrics and Test Methodology for the Verification of Multi-Antenna Reception Performance of NR User Equipment (UE)*, 3GPP document 38.827, V2.0.0, Jun. 2020. [Online]. Available: http://www.3gpp.org/

[10] "Preliminary LTE MIMO OTA test results using two-stage method," Proceeding of TSG-RAN WG4 Meeting, Agilent Technol., Shanghai, China, Tech. Rep. R4-112184, Apr. 2011.

[11] W. Yu *et al.*, "Radiated two-stage method for LTE MIMO user equipment," *IEEE Trans. Electromagn. Compat.*, vol. 56, no. 6, pp. 1691–1696, Dec. 2014.

[12] W. Fan *et al.*, "MIMO terminal performance evaluation with a novel wireless cable method," *IEEE Trans. Antennas Propag.*, vol. 65, no. 9, pp. 4803–4814, Sep. 2017.

[13] M. Berbeci, P. Pelland, and T. Leifert, "Challenges for the automotive industry on MIMO OTA testing," in *Proc. Antenna Mea. Tech. Associ. Sym. (AMTA)*, Newport, RI, USA, Dec. 2020, pp. 2–5.

[14] D. S. Baum *et al.*, "An interim channel model for beyond-3G systems: Extending the 3GPP spatial channel model (SCM)," in *Proc. IEEE 61st Veh. Technol. Conf.*, 2005, pp. 3132–3136.

[15] P. Kyösti, J. Meinilä, and L. Hentilä, "IST–4–027756 WINNER IID1.1.2 729 v.1.1: WINNER II channel models," WINNER II, Sarajevo, Bosnia and Herzegovina, Tech Rep D1.1.2 V1.1, 2007.

[16] H. Q. Ngo, M. Matthaiou, T. Q. Duong, and E. G. Larsson, "Uplink performance analysis of multicell MU-SIMO systems with ZF receivers," *IEEE Trans. Veh. Technol.*, vol. 62, no. 9, pp. 4471–4483, Nov. 2013.
[17] M. Kang and M.-S. Alouini, "Capacity of MIMO Rician channels," *IEEE Trans. Wireless Commun.*, vol. 5, no. 1, pp. 112–122, Jan. 2006.
[18] S. Alamouti, "A simple transmit diversity technique for wireless communications," *IEEE J. Sel. Areas Commun.*, vol. 16, no. 8, pp. 1451–1458, Oct. 1998.
[19] A. Forenza, M. R. McKay, A. Pandharipande, R. W. Heath, Jr., and I. B. Collings, "Adaptive MIMO transmission for exploiting the capacity of spatially correlated channels," *IEEE Trans. Veh. Technol.*, vol. 56, no. 2, pp. 619–630, Mar. 2007.
[20] H. N. M. Mbonjo, J. Hansen, and V. Hansen, "MIMO capacity and antenna array design," in *Proc. IEEE Global Telecom. Conf.*, Dallas, TX, USA, vol. 5, Nov. 2004, pp. 3155–3159.
[21] X. Chen, "Throughput modeling and measurement in an isotropic-scattering reverberation chamber," *IEEE Trans. Antennas Propag.*, vol. 62, no. 4, pp. 2130–2139, Apr. 2014.
[22] N. Prasad and M. K. Varanasi, "Outage theorems for MIMO block-fading channels," *IEEE Trans. Inf. Theory*, vol. 58, no. 7, pp. 2159–2168, Jul. 2006.
[23] R. Vaughan and J. Andersen, "Antenna diversity in mobile communications," *IEEE Trans. Veh. Technol.*, vol. 36, no. 4 pp. 149–172, Nov. 1987.
[24] X. Chen, W. Fan, P. Kyösti, L. Hentilä, and G. F. Pedersen, "Throughput modeling and validations for MIMO-OTA testing with arbitrary multipath," *IEEE Antennas Wireless Propag. Lett.*, vol. 17, no. 4, pp. 637–640, Apr. 2018.
[25] *Analysis of DUT pool 4 Test Results*, presented at the 3GPP TSGRAN WG4 Meeting #61, document R4-115655, Nokia, San Francisco, CA, USA, Nov. 2011.
[26] G. G. Raleigh and J. M. Cioffi, "Spatio-temporal coding for wireless communications," in *Proc. IEEE Global Telecom. Conf.*, London, U.K., vol. 3, Nov. 1996, pp. 1809–1814.
[27] H. Tataria, P. J. Smith, L. J. Greenstein, and P. A. Dmochowski, "Zero-forcing precoding performance in multiuser MIMO systems with heterogeneous Ricean fading," *IEEE Wireless Commun. Lett.*, vol. 6, no. 1, pp. 74–77, Feb. 2017.
[28] S. Serbetli and A. Yener, "Transceiver optimization for multiuser MIMO systems," *IEEE Trans. Signal Process.*, vol. 52, no. 1, pp. 214–226, Jan. 2004.
[29] G. J. Foschini and M. J. Gans, "On limits of wireless communication in a fading environment when using multiple antennas," *IEEE Wireless Pers. Commun.*, vol. 6, no. 3, pp. 311–335, Mar. 1998.
[30] *LTE Physical Layer*, 3GPP documnet TS 36201, V8.1.0, 2007. [Online]. Available: http://www.3gpp.org/
[31] *5G NR Overall Description Stage-2*, 3GPP document TS 38.300, V15.2.0, 2018. [Online]. Available: http://www.3gpp.org/
[32] R. B. Ertel *et al.*, "Overview of spatial channel models for antenna array communication systems," *IEEE Pers. Commun.*, vol. 5, no. 1, pp. 10–22, Feb. 1998.
[33] A. Klein and W. Mohr, "A statistical wideband mobile radio channel model including the directions-of-arrival," in *Proc. Int. Symp. Spread Spectr. Techn. Appl. (ISSSTA)*, Sep. 1996, pp. 102–106.
[34] J. Salo *et al.*, *MATLAB Implementation of the 3GPP Spatial Channel Model*, 3GPP, FR., document 25.996, 2005. [Online]. Available: http://www.tkk.fi/Units/Radio/scm
[35] A. F. Molisch, "Wideband spatial channel model in an urban cellular environments at 28 GHz," in *Wireless Communications*, 2nd ed. West Sussex, U.K.: Wiley, 2011, pp. 110–112.
[36] W. Fan, P. Kyösti, J. Ø. Nielsen, and G. F. Pedersen, "Wideband MIMO channel capacity analysis in multiprobe anechoic chamber setups," *IEEE Trans. Veh. Technol.*, vol. 65, no. 5, pp. 2861–2871, May 2016.
[37] P. S. Kildal *et al.*, "Threshold receiver model for throughput of wireless devices with MIMO and frequency diversity measured in reverberation chamber," *IEEE Antennas Wireless Propag. Lett.*, vol. 10, pp. 1201–1204, 2011.
[38] *Verification of Radiated Multi-Antenna Reception Performance of User Equipment*, 3GPP document 37.977, V1.0.0, 2013. [Online]. Available: http://www.3gpp.org/
[39] *StarMIMO: A MIMO Device End-to-End Test System*. Microwave Vision Group, FR. Accessed: Sep. 2018. [Online]. Available: https://www.mvg-world.com/
[40] *CMW Wideband Radio Communication Tester*. Rohde & Schwarz, Version 5.0. Accessed: Sep. 2019. [Online]. Available: https://www.rohde-schwarz.com/
[41] Y. Ji, W. Fan, G. F. Pedersen, and X. Wu, "On channel emulation methods in multiprobe anechoic chamber setups for over-the-air testing," *IEEE Trans. Veh. Technol.*, vol. 67, no. 8, pp. 6740–6751, Aug. 2018.
[42] J. Sui, Y. Dou, X. Mei, and K.-L. Wu, "Self-curing decoupling technique for MIMO antenna arrays in mobile terminals," *IEEE Trans. Antennas Propag.*, vol. 68, no. 2, pp. 838–849, Feb. 2020.
[43] *High Tack Pressure Sensitive Adhesive Tape: ECCOSORB SS Tapes*, Euro Technol., Concorezzo, Italy, 2018. [Online]. Available: https://www.euro-technologies.eu/en/product/eccosorb-ss-tapes/
[44] K.-H. Chen and J.-F. Kiang, "Effect of mutual coupling on the channel capacity of MIMO systems," *IEEE Trans. Veh. Technol.*, vol. 65, no. 1, pp. 398–403, Jan. 2016.
[45] X. Mei and K.-L. Wu, "How low does mutual coupling need to be for MIMO antennas," in *Proc. IEEE Int. Symp. Antennas Propag. USNC/URSI Nat. Radio Sci. Meeting*, Jul. 2018, pp. 1579–1580.

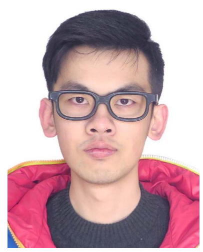

Xide Mei received the B.S. degree in electronic engineering from the University of Electronic Science and Technology of China, Chengdu, China, in 2015. He is currently pursuing the Ph.D. degree with The Chinese University of Hong Kong, Hong Kong.

His current research interests include antenna design, performance evaluation of terminal devices, and the design of multiple-input and multiple-output antenna arrays by incorporating wireless channel models.

Ke-Li Wu (Fellow, IEEE) received the B.S. and M.Eng. degrees from the Nanjing University of Science and Technology, Nanjing, China, in 1982 and 1985, respectively, and the Ph.D. degree from Laval University, Quebec, QC, Canada, in 1989.

From 1989 to 1993, he was a Research Engineer with McMaster University, Hamilton, ON, Canada. He joined COM DEV (now Honeywell Aerospace), Cambridge, ON, Canada, in 1993, where he was a Principal Member of Technical Staff. Since 1999, he has been with The Chinese University of Hong Kong, Hong Kong, where he is currently a Professor and the Director of the Radio frequency Radiation Research Laboratory. His current research interests include electromagnetic (EM)-based circuit domain modeling of high-speed interconnections, robot automatic tuning of microwave filters, decoupling techniques of multiple-input and multiple-output (MIMO) antennas, and the Internet-of-Things (IoT) technologies.

Dr. Wu is a member of the IEEE MTT-8 Subcommittee. He was a recipient of the 1998 COM DEV Achievement Award and the Asia-Pacific Microwave Conference Prize Twice in 2008 and 2012, respectively. He was an Associate Editor of the IEEE TRANSACTIONS ON MICROWAVE THEORY AND TECHNIQUES from 2006 to 2009.